AD-A159 915 THE EFFECTS OF HYDROSTATIC PRESSURE ON OPTICAL FIBERS (FISCAL YEAR 1983 REPORT)(U) NAVAL OCEAN SYSTEMS CENTER SAN DIEGO CA N KAMIKAWA APR 85 NOSC/TR-1023 1/1

UNCLASSIFIED F/G 20/6 NL

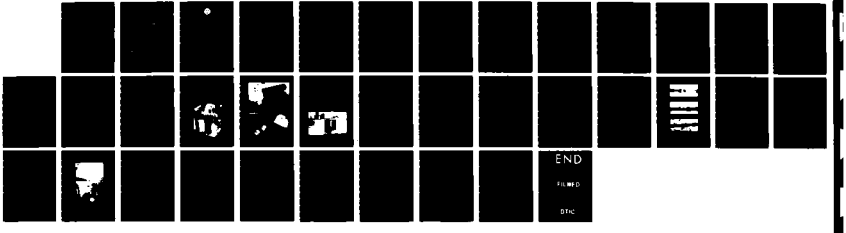

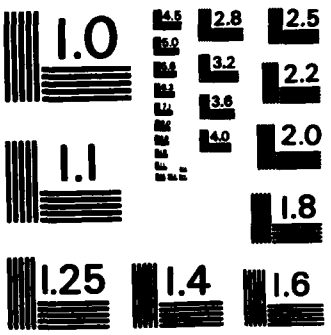

TR 1023

(12)

TR 1023

Technical Report 1023
April 1985

THE EFFECTS OF HYDROSTATIC PRESSURE ON OPTICAL FIBERS (FY 83 REPORT)

Neil Kamikawa

Naval Ocean Systems Center
San Diego, California 92152-5000

NAVAL OCEAN SYSTEMS CENTER SAN DIEGO, CA 92152

AN ACTIVITY OF THE NAVAL MATERIAL COMMAND

F. M. PESTORIUS, CAPT, USN
Commander

R.M. HILLYER
Technical Director

ADMINISTRATIVE INFORMATION

The work reported herein was sponsored by the NOSC Independent Research and Independent Exploratory Development Program and conducted during FY 83 under 62766N-F66512-ZE07.

Released by
F. P. Armogida, Head
Advanced F/O Systems Branch

Under authority of
J. D. Hightower, Head
Advanced Systems Division

AS

UNCLASSIFIED
SECURITY CLASSIFICATION OF THIS PAGE

REPORT DOCUMENTATION PAGE

1a. REPORT SECURITY CLASSIFICATION UNCLASSIFIED	1b. RESTRICTIVE MARKINGS
2a. SECURITY CLASSIFICATION AUTHORITY	3. DISTRIBUTION/AVAILABILITY OF REPORT Approved for public release; distribution unlimited.
2b. DECLASSIFICATION/DOWNGRADING SCHEDULE	
4. PERFORMING ORGANIZATION REPORT NUMBER(S) NOSC TR 1023	5. MONITORING ORGANIZATION REPORT NUMBER(S)
6a. NAME OF PERFORMING ORGANIZATION Naval Ocean Systems Center 6b. OFFICE SYMBOL (If applicable) Code 5334	7a. NAME OF MONITORING ORGANIZATION
6c. ADDRESS (City, State and ZIP Code) San Diego, CA 92152-5000	7b. ADDRESS (City, State and ZIP Code)
8a. NAME OF FUNDING/SPONSORING ORGANIZATION 8b. OFFICE SYMBOL (If applicable)	9. PROCUREMENT INSTRUMENT IDENTIFICATION NUMBER
8c. ADDRESS (City, State and ZIP Code)	10. SOURCE OF FUNDING NUMBERS PROGRAM ELEMENT NO. 62766N; PROJECT NO. F66512; TASK NO. ZE07; Agency Accession DN387 502

11. TITLE (Include Security Classification)
THE EFFECTS OF HYDROSTATIC PRESSURE ON OPTICAL FIBERS
(FY 83 Report)

12. PERSONAL AUTHOR(S)
Neil Kamikawa

13a. TYPE OF REPORT	13b. TIME COVERED	14. DATE OF REPORT (Year, Month, Day)	15. PAGE COUNT
Research	FROM Oct 82 TO Oct 83	April 1985	31

16. SUPPLEMENTARY NOTATION
(Cert Rpt)

17. COSATI CODES

FIELD	GROUP	SUB-GROUP

18. SUBJECT TERMS (Continue on reverse if necessary and identify by block number)
Fiber optic coatings; Coating defects; Buckling behavior; Undersea data link; Transmission quality;

19. ABSTRACT (Continue on reverse if necessary and identify by block number)

A pressure model is presented that explains how hydrostatic pressure can increase losses in polymer-coated optical fibers. Pressure tests on defectively coated fibers are described. Development of a model that comprehends low temperature as well as high pressure is recommended.

20. DISTRIBUTION/AVAILABILITY OF ABSTRACT	21. ABSTRACT SECURITY CLASSIFICATION
[X] UNCLASSIFIED/UNLIMITED [ ] SAME AS RPT [ ] DTIC USERS	UNCLASSIFIED

22a. NAME OF RESPONSIBLE INDIVIDUAL	22b. TELEPHONE (Include Area Code)	22c. OFFICE SYMBOL
Neil Kamikawa	(808) 254-4355	Code 5334

DD FORM 1473, 84 JAN

83 APR EDITION MAY BE USED UNTIL EXHAUSTED
ALL OTHER EDITIONS ARE OBSOLETE

UNCLASSIFIED
SECURITY CLASSIFICATION OF THIS PAGE

(polymer-coated)

FOREWORD

This report stems from a NOSC Independent Exploratory Development project tasked to investigate experimentally the effects of deep-ocean hydrostatic pressure on optical fiber transmission. In FY 83 it was concluded that optical fibers could be designed so that pressure equivalent to a 6-km (20,000-ft) ocean depth does not increase fiber losses. This conclusion was based on an axial compression model and experiments performed on polymer-coated graded-index fibers. Defects in the coating were identified as additional causes of loss increase. Defectively coated fibers exhibited very large excess loss in hydrostatic environments. It was recommended that FY 84 efforts should investigate the combined effects of high pressure and low temperature (i.e., typical deepsea conditions) on optical fiber transmission.

This report summarizes work performed in FY 83. A pressure model and fiber and coating material experiments are described and conclusions and recommendations stated. → Keywords: (to p. A)

CONTENTS

ILLUSTRATIONS

TABLES

INTRODUCTION

Researchers (References 1, 2) have measured large loss increases in polymer-coated fibers caused by hydrostatic pressure. This is a potentially serious problem for long-haul undersea data links. Pressure-induced excess losses threaten these links by degrading fiber transmission quality and reducing system reliability. For example, a 0.1-dB/km loss increase caused by pressure extrapolates to a total excess loss of 5 dB in a 50-km link. Five dB of excess loss is dangerously close to typical loss safety margins for error-free transmission in long-haul links.

Cable manufacturers solved the pressure problem for commerical applications by isolating the fiber from hydrostatic environments. This is usually done by using a metallic sheath or armor on the outer cable layers. The resultant cable is too large for many military applications requiring unique cable deployment schemes. Rapidly deployed trunks and tethers for weapons, for example, require lightweight, minimum-diameter cables.

In the research conducted in FY 83, it was found that it was unnecessary to isolate the fibers from pressure. This conclusion was based on experimental investigations into two modes of fiber loss increase caused by hydrostatic pressure. The first was axial compression of the coated glass, which can lead to its buckling. The model assumed a defect-free coating. With this model, fiber coatings can be designed to minimize axial compression and prevent buckling. The second mode was microbending triggered by defects in the coating. This effect was unpredictable and difficult to model. The loss increases observed (References 1, 2) were probably due to defects contained in the fiber.

A pressure model that explains how pressure can increase losses in polymer-coated fibers is presented first in this report. The model assumes defect-free coatings. This is followed by a description of pressure tests performed on defectively coated fibers. Large loss increases were measured. The last section summarizes our conclusions. It also contains a recommendation for development of a high-pressure, low-temperature model that will provide a more accurate simulation of sea-floor conditions.

AXIAL COMPRESSION MODEL

INTRODUCTION

Excess loss in an optical fiber is the attenuation increase that it suffers when moved from an unstressed environment into an environment that applies any or all of a number of possible stresses. Fiber loss in unstressed conditions is determined by intrinsic fiber properties. These include Rayleigh scattering, absorption, and geometric imperfections. Losses can increase in a hydrostatic environment when a coated fiber buckles as a result of pressure-induced axial compressive stresses. The fiber bends helically with a bend radius that is determined by the dimensions of the glass fiber and its coating and the compressive forces. As the compressive forces increase, the bend radius of the helix decreases. Fiber losses increase as optical energy, which propagates normally in a straight fiber, now scatters at these small-radii bends.

A model based on axial compression was developed to explain buckling in polymer-coated fibers. It assumed that the coating was free of defects. This model can be used to predict the pressure levels that are large enough to cause buckling. Conversely, it can be used to design fiber coatings so that the fiber will not buckle at operating depths in the ocean. This section desribes this model. The mathematical analysis of the model is explained first. This is followed by an outline of experiments performed to validate the model.

ANALYSIS

Theoretical calculations show that polymer-coated fibers shrink radially and longitudinally in hydrostatic environments. The fibers will buckle if the compressive strain is greater than a threshold buckling strain. The compressive strains in fibers chosen for analysis and testing were less than the buckling strain up to a peak of 700 kg/cm^2 (10,000 psi). Therefore, pressure-induced loss increases in these fibers were not anticipated.

The axial compression of an uncoated fiber can be computed simply from Hooke's Law:

$$e' = \frac{-P}{3B_1} \quad , \tag{1}$$

where P is pressure and B_1 is the bulk modulus of glass. If the fiber is coated with a polymer (most commercial fibers are), the polymer shrinks more than the glass and exerts an additional compressive strain in the fiber. Equation (2) relates this additional axial compressive strain in fibers to the properties of the fiber and its coating (see appendix and Reference 2 for derivation):

$$\Delta e = \int \frac{(1/B_1 - 1/B_3)}{3\left[1+\frac{S_1E_1}{S_3E_3}\right]}\,dp \quad . \tag{2}$$

B is the bulk modulus, E is the Young's modulus, and S is the cross-sectional area. The subscripts 1 and 3 refer to the fiber and its outer coating, respectively, as shown in Table 1. The fiber's inner coating (denoted by the subscript 2) was ignored in the calculation because its modulus was at least two orders of magnitude less than the outer coating. Its contribution to the strain was insignificant.

According to Equation (2), the additional strain in these fibers is directly proportional to pressure and the difference between material compressibilities (reciprocal of bulk modulus). Since polymers have lower bulk moduli than glass ($B_3 < B_1$), Δe is negative and compressive. Equation (2) also shows that fibers with thicker coatings (S_3) will have greater strains.

If Δe is greater than a threshold strain, e_b, the fiber buckles (Reference 3). The theoretical buckling strain is:

$$e_b = \sqrt{E_2/\pi E_1} \quad . \tag{3}$$

When the fiber buckles, it forms a helix as shown schematically in Figure 1.

Table 1 describes the polymer-coated fibers that were analyzed and tested. Nylon-12 and Hytrel-7246 coated fibers were chosen because these fibers are commonly used in undersea systems, and the physical properties of the coatings are available from manufacturers. UV-cured acrylate-coated fibers also were tested, but they are not included in the analysis that follows. Vendors that use UV-cured acrylates consider the physical properties of these fibers highly proprietary and would not release any data. The analysis and testing applies to single-mode fibers as well as multimode fibers.

Fibers A-1 and A-2 are similar (from the same manufacturer), but the diameter of the outer coating is larger in fiber A-2. Fibers B-1 and B-2 are also similar, except that the outer coating diameter and numerical aperture (NA) are larger in B-2.

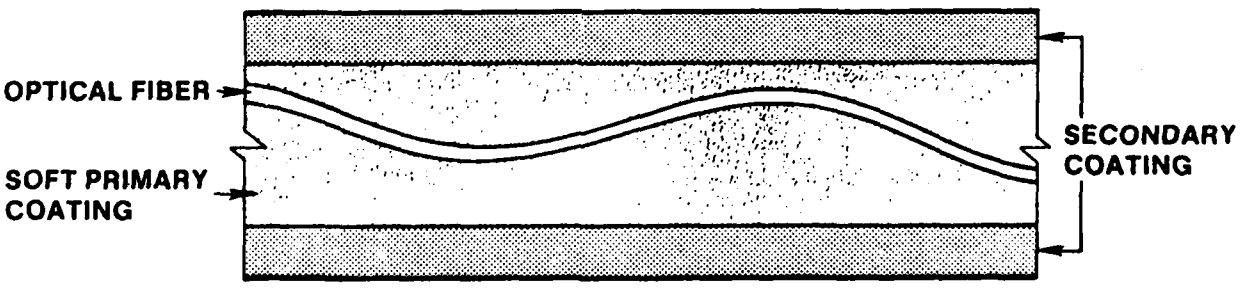

Figure 1. Buckling in a polymer-coated optical fiber.

Table 1. Description of fibers analyzed and tested (a is thermal expansion coefficient).

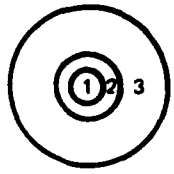

Fiber cross section (not drawn to scale)

LAYER	FIBER A-1	FIBER A-2	FIBER B-1	FIBER B-2
1	VAD multimode NA = 0.20 Core dia. = 0.050 mm OD = 0.125 mm Area = 0.0123 mm^2 a = $3X10^{-7}$ mm/mm/°C	same as fiber A-1	MCVD multimode NA = 0.22 Core dia. = 0.050 mm OD = 0.125 mm Area = 0.0123 mm^2	MCVD multimode NA = 0.26 Core dia. = 0.050 mm OD = 0.125 mm Area = 0.0123 mm^2
2	Silicone resin OD = 0.3 mm Area = 0.0584 mm^2 a = 10^{-4} mm/mm/°C	Silicone resin OD = 0.4 mm Area = 0.1134 mm^2	Silicone resin OD = 0.3 mm Area = 0.0584 mm^2	Silicone resin OD = 0.3 mm Area = 0.0584 mm^2
3	Nylon-12 OD = 0.5 mm Area = 0.1257 mm^2 a = 10^{-4} mm/mm/°C	Nylon-12 OD = 0.9 mm Area = 0.5105 mm^2	Hytrel-7246 OD = 0.5 mm Area = 0.1257 mm^2 a = $2X10^{-4}$ mm/mm/°C	Hytrel-7246 OD = 1.0 mm Area = 0.7147 mm^2
FIBER LENGTH	660 m	557 m	562 m	550 m

If the physical properties of the coating and fiber are known as a function of pressure, they can be used in Equation (2) to calculate the axial compressive strain. This strain can be compared to the buckling strain in Equation (3) to check for buckling at the anticipated pressure. However, there are very few data on the behavior of polymers as a function of hydrostatic pressure. To obtain such data, the Aerospace Corp. was tasked to characterize the coating materials. Drs. Bob Fillers and Sherrie Zacharius of Aerospace Corp. estimated that polymers become glasslike under pressure (see Reference 4) and their bulk modulus increases. They estimated that the bulk and Young's moduli increase by a factor of about two at 700 kg/cm^2 (10,000 psi) from their values at atmospheric pressure. These estimates and known zero-pressure values for Nylon-12, Hytrel-7246, and glass are listed in Table 2.

In an independent test, Mr. Mike Kono of NOSC Code 9421 measured the bulk modulus of the same polymers at 700 kg/cm^2. His results are also listed in Table 2. The bulk moduli estimated by Aerospace and measured by Kono are reasonably close.

Although the moduli at only 0 and 700 kg/cm^2 are known (instead of as continuous functions of pressure), the fiber compressive strain can be calculated approximately by means of Equation (2). The following approximations simplify the calculations:

(a) Assume the bulk and Young's moduli for Nylon-12 and Hytrel-7246 vary linearly with pressure between 0 and 700 kg/cm^2.

(b) Use the zero-pressure moduli for glass and assume it does not change over the entire pressure range.

The computed strain values are plotted in Figures 2 and 3 for fibers A-1, A-2, B-1 and B-2.

The buckling strain for these fibers is between -0.0030 and -0.0042. This is calculated using Equation (3). E_2, Young's modulus for the silicone resin coating, is about 0.1 to 0.2 kg/mm^2 at ambient (i.e., sea-level) conditions. At high pressures it is assumed to be 0.2 to 0.4 kg/mm^2, or twice the ambient values. The strains of all of the fibers are less than the buckling strains. Therefore, loss increase due to buckling is not expected at pressures up to 700 kg/cm^2.

EXPERIMENTAL APPROACH

Pressure experiments performed on fibers A-1, A-2, B-1 and B-2 (shown in Table 2) verify the axial compression model. The results show that the fibers experience axial compressive strains predicted by Equation (2). No loss increase due to buckling up to 700 kg/cm^2 occurs in these fibers because the strains are less than the computed buckling strain.

Table 2. Young's modulus and bulk modulus for coating and glass. All units are in kg/mm^2 (1 kg/mm^2 = 1422 psi).

@ Ambient (sea-level) Conditions

	Nylon-12	Hytrel-7246	Glass
Young's Modulus	100	21	7300
Bulk Modulus	830	342	3700

@ Pressure = 7 kg/mm^2 (10,000 psi)

	Nylon-12	Hytrel-7246	Glass
Young's Modulus	200 (Aerospace)	42 (Aerospace)	7300
Bulk Modulus	1758 (Kono) 1688 (Aerospace)	1125 (Kono) 682 (Aerospace)	3700

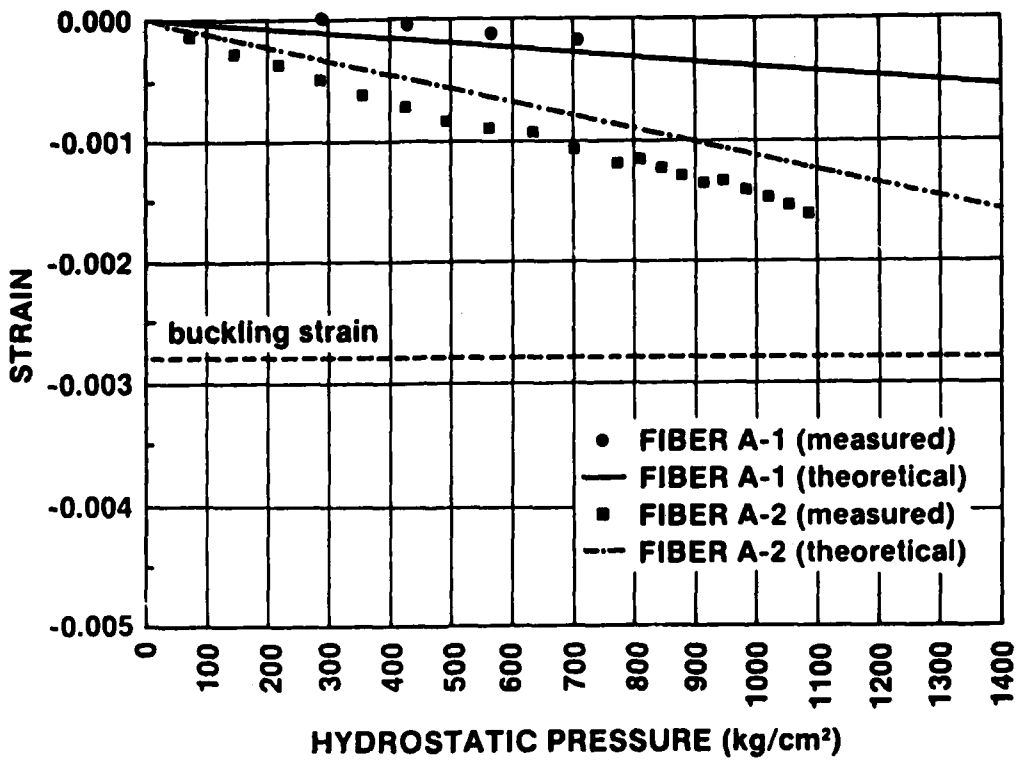

Figure 2. Strain vs pressure in fibers A-1 and A-2.

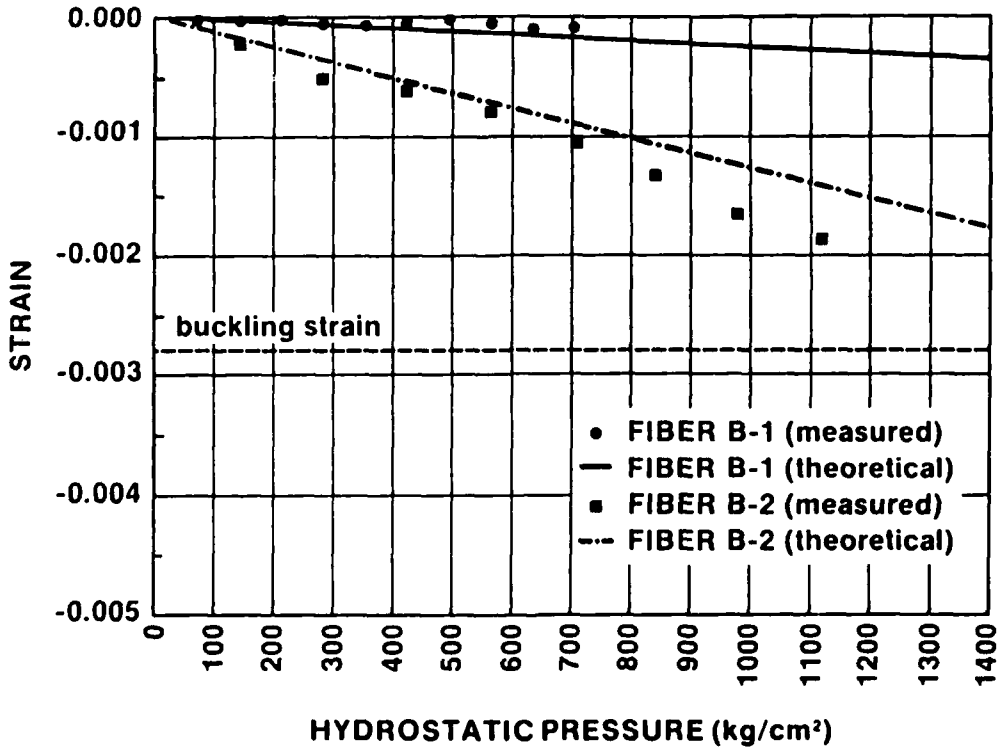

Figure 3. Strain vs pressure in fibers B-1 and B-2.

Instrumentation

Test Setup. To experimentally characterize the effects of hydrostatic pressure on the optical fibers, 500- to 600-m sample lengths of the fibers were pressure tested in a vessel consisting of a 16-in. projectile filled with water. One sample was tested at a time. The ends of the samples were brought out of the projectile through fiber optic penetrators so that optical measurement equipment could be used to evaluate fiber transmission (loss increase and strain) while pressure was applied to the fiber. The setup is shown schematically in Figure 4. The 16-in. projectile is shown in Figure 5. The pressure in the projectile was controlled from the panel (also shown in Figure 5).

Care was taken to ensure that loss increase or axial strain in the fibers was caused by hydrostatic pressure only. Each fiber sample was level-wound (no cross-overs) onto a 20-cm-OD mandrel which fit into the projectile. The fibers were wound under tension to keep each wind in place, but the tension was relieved after the mandrel was partially collapsed prior to insertion into the projectile. The mandrel is shown in Figure 6. The ends of the samples were led out of the projectile through penetrators as shown in Figure 7. The penetrators were tested up to 700 kg/cm^2 and no fiber loss inside the penetrator was observed. Figure 8 shows the cross section of the penetrator.

Excess Loss Measurement. To measure loss increase (excess loss) in the pressurized fiber, backscatter was measured with an optical-time-domain reflectometer (OTDR). Distribution of fiber loss can be evaluated with the OTDR. In this method, the fiber intrinsic loss is measured before pressure is applied to the fiber. Then the measurement is repeated after pressure is applied. The difference between the two measurements is the excess loss. A Laser Precision Co. (Model TD-9901) OTDR with a 0.82-μm laser (shown in Figure 9) was used in the tests. Faults or microbends could be localized to within $\pm$4 m. The TD-9901 was also equipped with a box-car averager so that optical power backscattered from any point along the fiber length could be averaged over 1,000 or 10,000 data samples. The 1,000-samples-per-point averaging was used in the tests. This type of averaging improves optical signal-to-noise and allows a $\pm$0.1-dB loss resolution.

Strain Measurement. Axial strain in fibers was measured by observing phase changes in the optical transmission of an RF intensity-modulated laser signal. (The method is described in Reference 5.) The schematic of the strain measurement is shown in Figure 10. A 1.3-μm laser was intensity-modulated by an RF oscillator and launched into the fiber under test inside the pressure vessel (16-in. projectile). The fiber output was detected by an InGaAs PIN photodiode and amplified. A vector voltmeter (VVM) measured the phase difference in the electrical signals between channels A and B. This phase difference was due to the delay of the signal through the laser, test fiber, and detector/amplifier. If the fiber was not stressed, the phase difference remained constant to within $\pm$3 deg over a period of several hours. When the fiber was compressed as pressure was applied, the signal delay decreased, and the VVM indicated a change in signal phase. This technique gives a $\pm$0.01% uncertainty in a 0.1% measured strain.

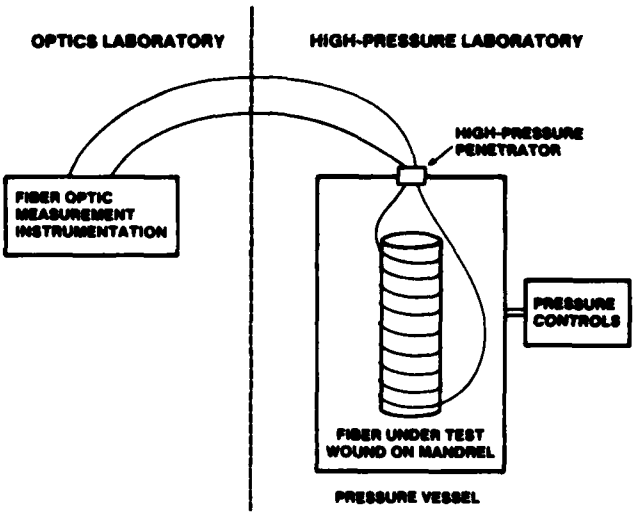

Figure 4. Pressure test setup.

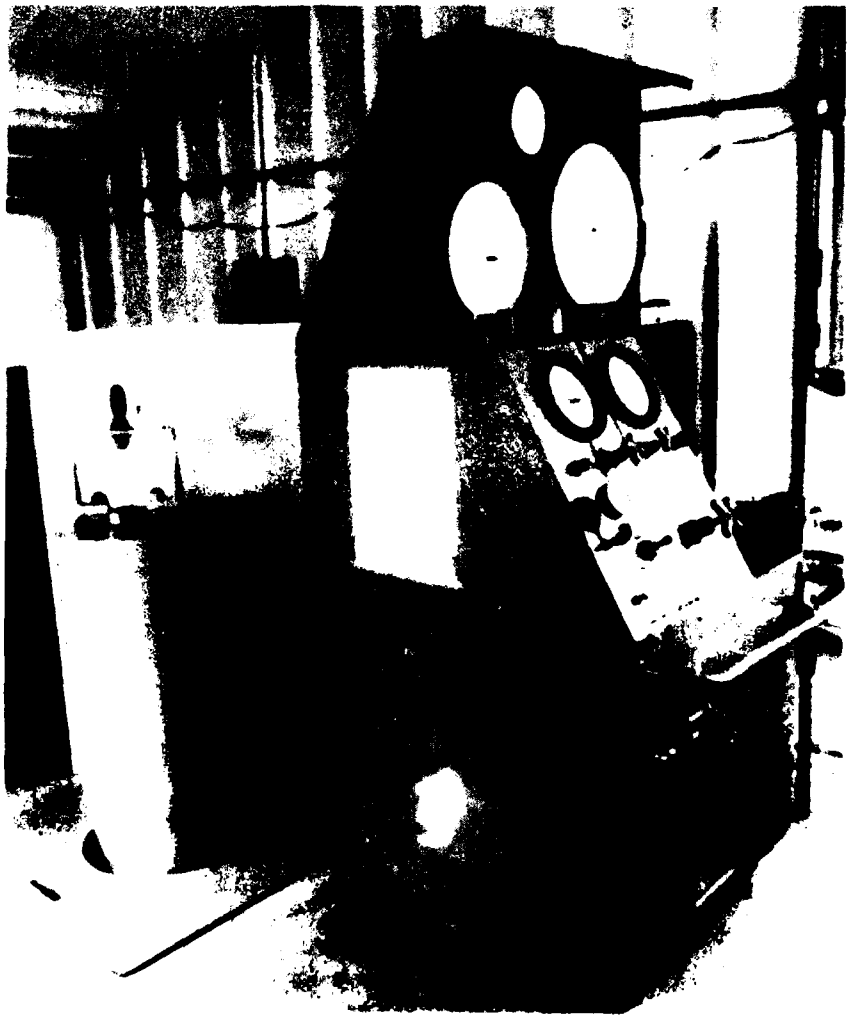

Figure 5. Pressure vessel (16-in. projectile) and control console.

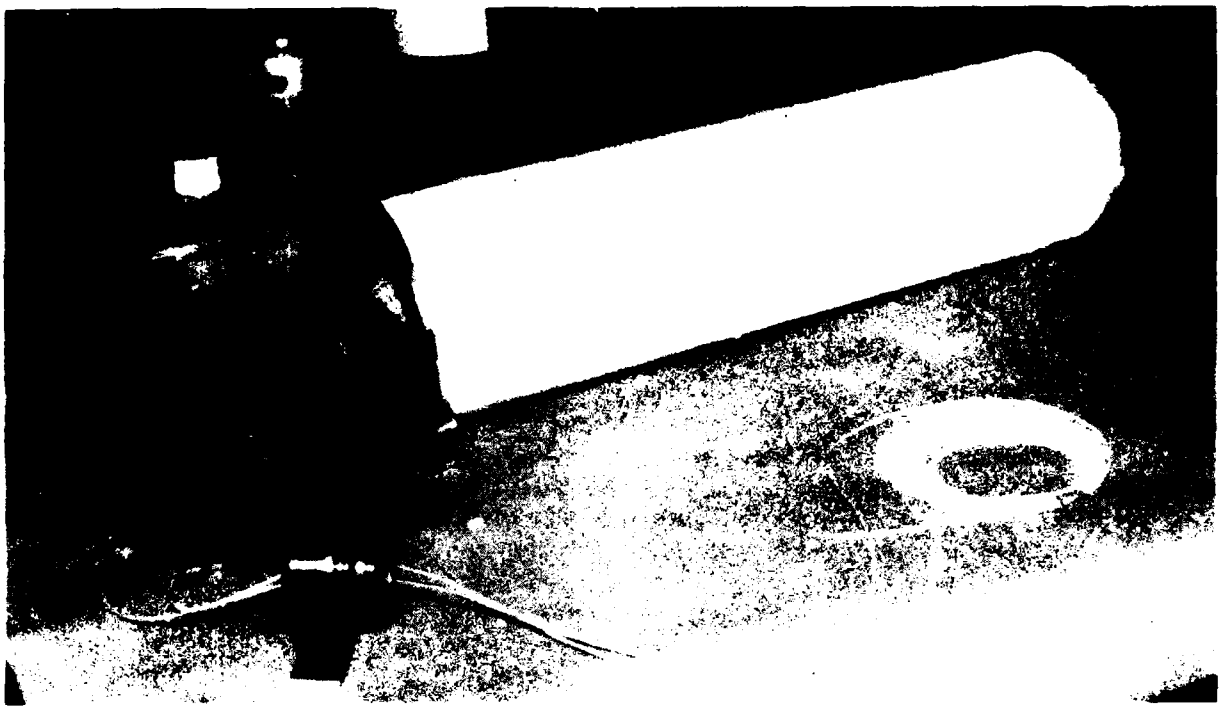

Figure 6. Fiber level wound on 20-cm-OD mandrel.

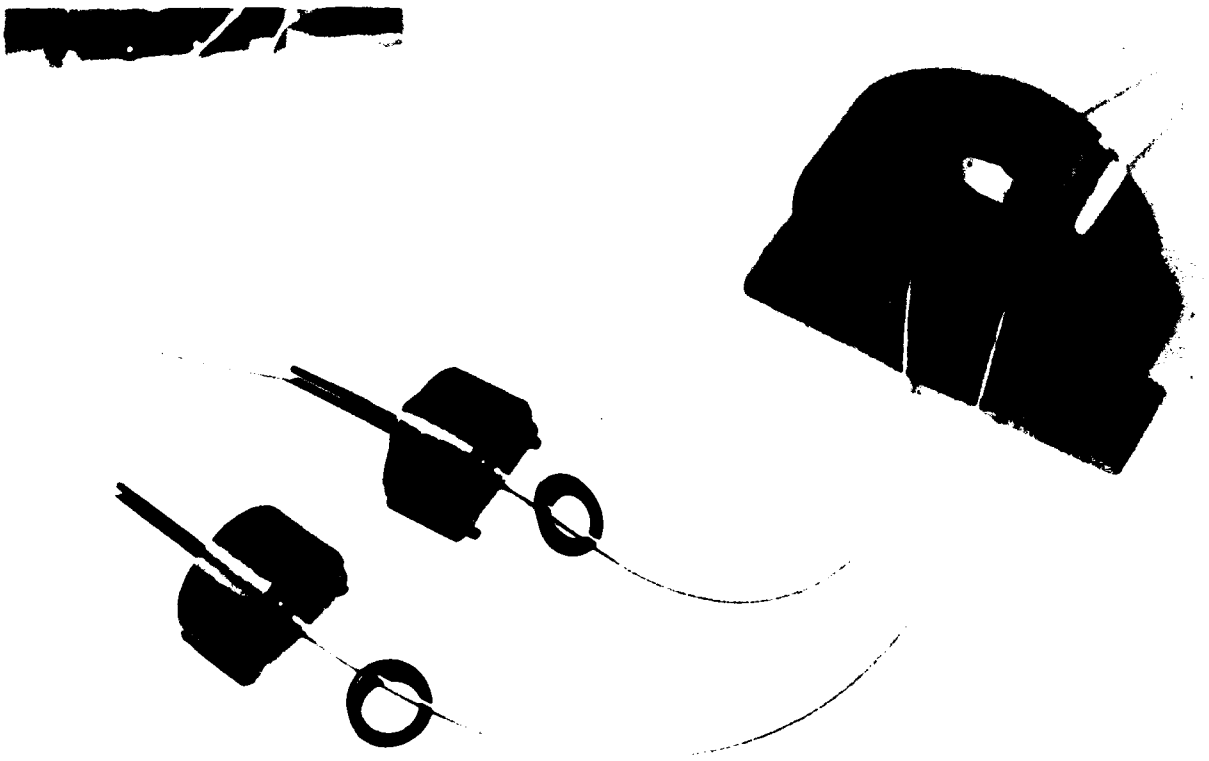

Figure 7. High-pressure fiber optic penetrators.

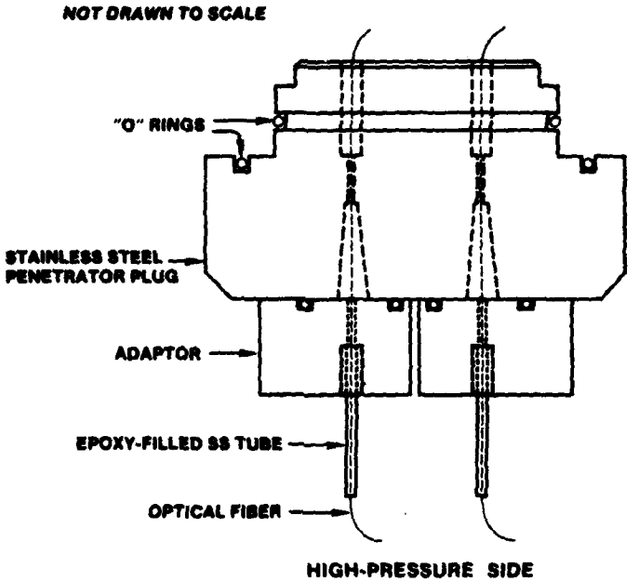

Figure 8. High-pressure penetrator cross section.

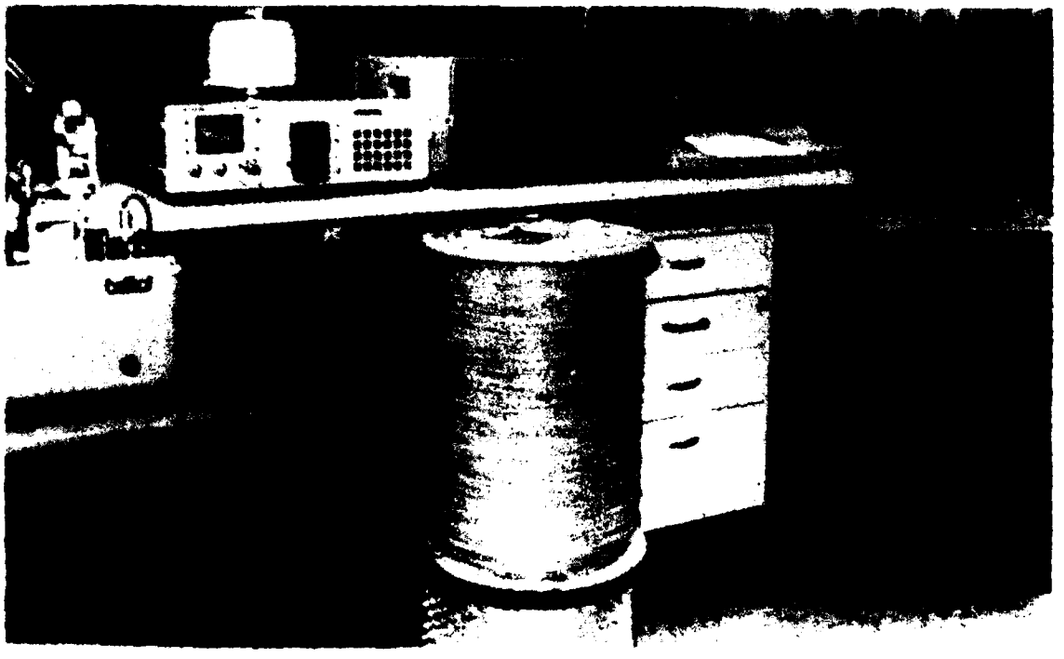

Figure 9. OTDR and data acquisition equipment.

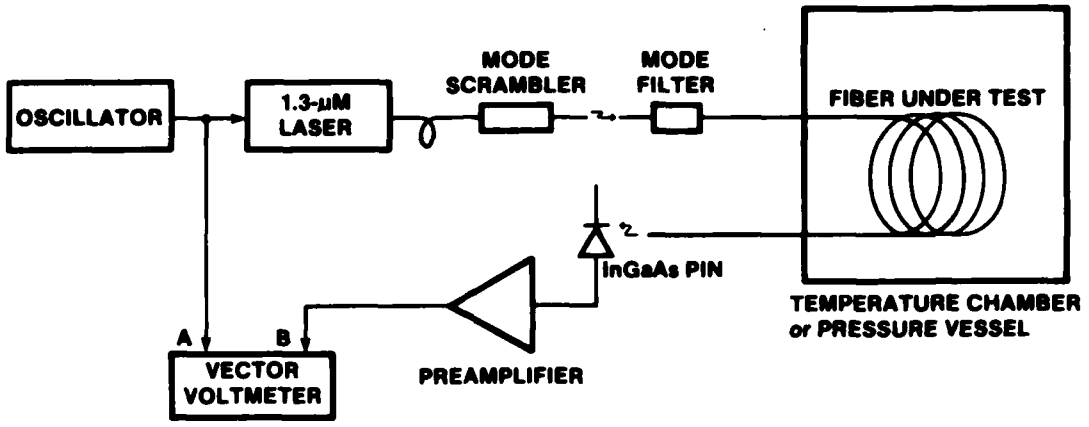

Figure 10. Optical fiber strain measurement system.

Proof of Measurement Technique

The value of the strain measurement technique to explain fiber behavior in adverse environments was initially proven in a temperature test. The relative compressive strains in fibers A-1 and A-2 were measured as the temperature of the fiber was cycled between -60 and +70°C. This was followed by excess loss measurements. Temperature tests were chosen because the model for fiber behavior in a varying temperature environment was understood and documented (Reference 6). Refining the strain measurement technique was easier in a temperature test.

Figure 11 shows the relative compressive strains in fibers A-1 and A-2 as a function of temperature. (The strains are relative to fiber length at room temperature.) The close agreement between the theoretical and measured strains indicates that the strain measurement technique is feasible.

The theoretical temperature-induced strains were computed from the model in Reference 6:

$$\Delta e = (a_3 - a_1) \int \frac{S_3 E_3}{S_1 E_1 + S_2 E_2 + S_3 E_3} \, dT \quad . \qquad (4)$$

S is the cross-sectional area, a is the thermal expansion coefficient, E is the Young's modulus, and T is temperature. S and a for fibers A-1 and A-2 are listed in Table 1. The Young's modulus for Nylon-12 (layer 3) and silicone resin (layer 2) as functions of temperature are shown in Figure 12. The buckling strain for these fibers, e_b, is about -0.0028 according to Equation (3) for $E_2 = 0.18$ kg/mm^2.

According to the temperature model in Equation (4) and computations in Figure 11, fiber A-1 should not exhibit buckling-induced loss increases because the strain is less than -0.0028 for temperatures greater than -60°C. However, fiber A-2 should buckle at temperatures less than -35°C. As an additional check on the model and strain measurement technique, the losses in both fibers were monitored as the fiber temperature was reduced to -60°C. The results are shown in Figure 13. Fiber A-1 exhibited no loss increase, but the

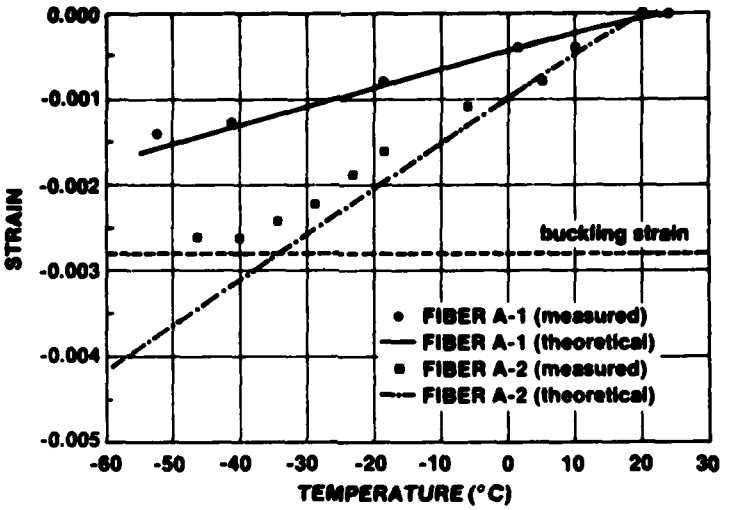

Figure 11. Strain vs temperature in fibers A-1 and A-2.

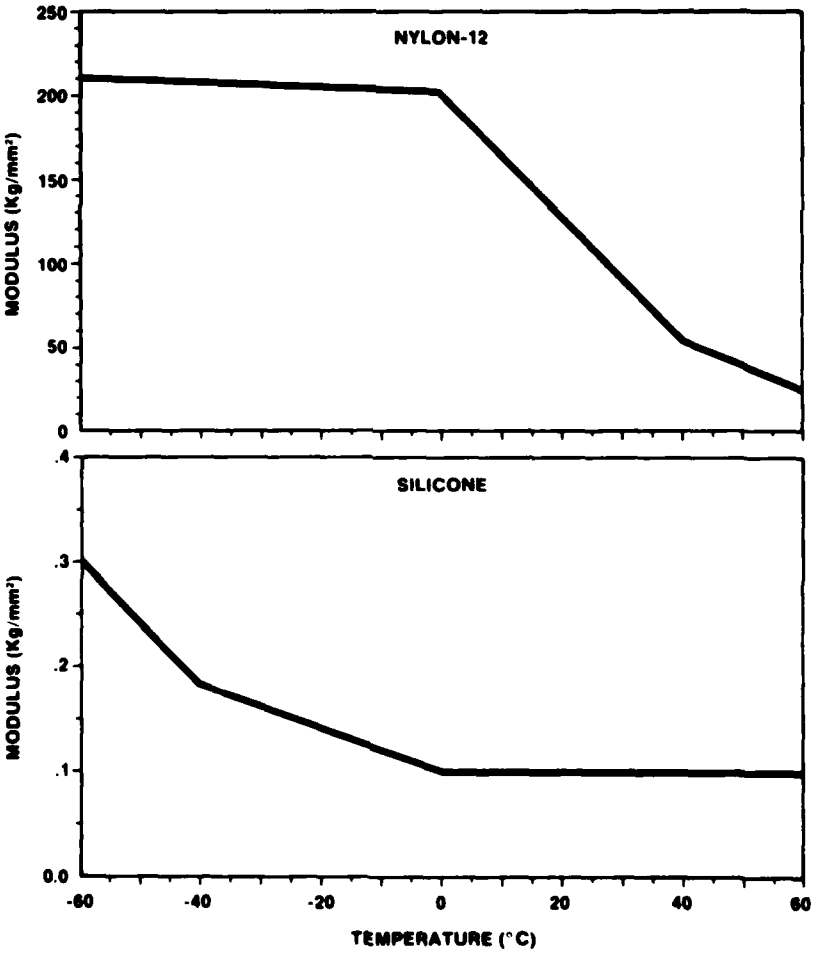

Figure 12. Young's Moduli for Nylon-12 and silicone resin.

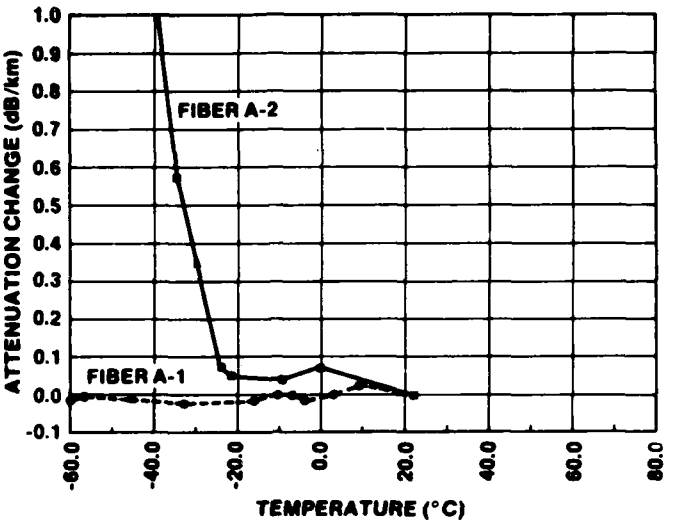

Figure 13. Attenuation change vs temperature in fibers A-1 and A-2.

loss in fiber A-2 increased sharply below -25°C. Fiber A-2 buckled at a slightly higher temperature than predicted because these fibers can have residual compressive strains as much as -0.001 set into the fiber when the coating is applied. (See Reference 7.)

Results of the Pressure Experiments

The lengthwise compressive strain and excess loss in the fibers described in Table 1 were measured as a function of pressure up to at least 700 kg/cm^2. The objective of the tests was to verify the pressure/strain model explained in Equation (2).

Measured strains in fibers A-1 and A-2 are plotted as functions of hydrostatic pressure in Figure 2. These "additional" strains are caused by the coating and do not include axial strains in an uncoated fiber described by Equation (1). These measurements were made at a wavelength of 1.3 μm using the technique described earlier. The measured strains are relative to the fiber length at atmospheric pressure. The lengths of the fibers tested are listed in the last row of Table 1. As predicted by Equation (2), the compressive strain in fiber A-2 was larger because its outer coating was thicker. Figure 3 shows the measured axial strains in fibers B-1 and B-2. Again, the strain in fiber B-2 was larger than in B-1 because it had a thicker outer coating.

The agreement between measured and calculated strain shows that Equation (2) is a valid pressure model for polymer-coated fibers. Strains in fibers A-1 and B-1 are small and near the strain resolution limit of the $\pm$0.01% measurement system. Strains in fibers A-2 and B-2 are much larger, but still less than the buckling strain for pressures less than 700 kg/cm^2.

To prove that these fibers do not buckle, excess loss measurements were made on the fibers. When the compressive axial strain in the fiber exceeds the buckling strain, the fiber forms a helix as explained in Reference 3 and shown in Figure 1. The helix has a characteristic pitch angle with the central axis and a radius of curvature determined by the dimensions of the fiber and coatings. If fiber A-1, A-2, B-1, or B-2 buckles, the radius of curvature of the fiber helix ranges from 2 to 6 cm. The curvature values were calculated for a 0.125-mm-OD fiber in Reference 3. These bends are small enough to cause relativistic scattering losses, which can be detected on an OTDR.

The optical backscatter in each fiber was measured prior to testing and repeated as the pressure was increased in 70-kg/cm^2 increments. No loss change greater than the resolution of the OTDR ($\pm$0.1 dB) could be detected. The OTDR measurements proved that the fibers did not buckle.

DEFECTIVE COATING

INTRODUCTION

Defective coatings were found to be a major cause of fiber buckling and microbending in hydrostatic pressure environments. Fibers with coating impurities, bubbles, or poor concentricities and eccentricities buckle in hydrostatic environments because axial and radial forces in the coating do not balance. In the previous section, it was shown that fibers without coating defects shrink axially until compression reached the buckling strain. At pressures for which the axial compressive strains were less than the threshold buckling strain, no buckling and microbending losses were detected. However, fibers with defective coatings can exhibit very large microbending losses at pressures much less than those which trigger buckling. This more complex phenomenon is explained below.

A fiber with a defective plastic coating and another with an epoxy/S-glass jacket were pressure tested. Large pressure-induced excess losses were observed in both. This section explains results from pressure tests performed on the two fibers. The first fiber was coated with silicone resin and Hytrel-7246 containing numerous bumps and areas where the coating "necked down" to expose bare fiber. The following observations were made during pressure tests on this fiber: (a) pressure-induced excess losses were casued by microbending at the defects; (b) losses in the fiber increased only during the initial application of pressure; (c) these excess losses gradually dissipated as stresses in the fiber relaxed at high pressure; and (d) water migrated along the fiber/coating interface.

The second fiber exhibited large excess losses, even under pressure as low as 70 kg/cm^2 (1,000 psi). It was coated with silicone resin and an epoxy/S-glass ruggedizing jacket. Stresses in the coating which caused microbending eventually relaxed, and excess losses dissipated in a long-term soak at high pressure.

COATING "NECK DOWNS" AND BUMPS

Test Description

This test proved that defectively coated fibers suffered from excess losses. It also demonstrated the need for good quality control in fiber coatings. Table 1 describes the B-1 fiber tested. The Hytrel-7246 coating contained many "neck downs" and bumps which were easily detected by the unaided eye. Each defect was 1 to 5 mm in length and occurred randomly along the length of the fiber. Typical "neck downs" and bumps are displayed in Figure 14.

Figure 14. Coating defects.

In order to correlate coating defects with microbending loss, the distance of these "neck downs" and bumps from the fiber ends was measured. This was done while winding the fiber onto the mandrel (shown in Figure 6) for testing. Microbending loss in the pressurized fiber was detected and localized with the 0.82-μm OTDR. The fiber was pressure tested in the 16-in. projectile shown in Figure 5.

Pressure Test Results

The test consisted of three pressure cycles as shown in the pressure-versus-time profile in Figure 15. Two low-pressure cycles preceded the pressure excursion up to 700 kg/cm^2 (10,000 psi) and an 18-day soak. In the 700-kg/cm^2 cycle, the pressure was raised in 70-kg/cm^2 increments. The pressure was returned to zero after the eighteenth day.

Figures 16 and 17 display the backscatter recorded by the OTDR during various segments of the pressure cycles. The relative order of these OTDR measurements is shown in Figure 15. Trace A was taken prior to the test and used as a baseline (at atmospheric pressure) for comparison with data recorded at other pressures. It is displayed in both Figures 16 and 17.

The asterisks in Figure 16 indicate the location of "neck downs" and bumps in the coating. The microbending losses in the fiber under pressure occur within measurement uncertainty of the defects. A 20-ns pulse width emitted by the OTDR caused at least a $\pm$4-m uncertainty in distance measurement. Measurement of the distance of each defect made by test personnel while the fiber was being wound onto the mandrel was probably equally uncertain.

The largest loss increase occurred during the smallest, but first, pressure cycle as shown by trace B in Figure 16. The fiber appeared to be "shocked" in the first cycle and virtually unaffected by the following pressure cycles even though the pressures were much greater. When the pressure was held at 700 kg/cm^2 (10,000 psi) for about a day, the stresses in the fiber relaxed and the loss returned to its original baseline value. Fiber monitoring with the OTDR continued for 18 days while the fiber remained pressurized at 700 kg/cm^2. No change in fiber loss was detected during this period.

During the pressure excursion from 0 to 700 kg/cm^2, droplets of water were observed at the fiber ends. Water probably entered the fiber between the glass and coating interface at defect sites and migrated to the fiber ends located outside the pressure chamber. This observation suggests that water intrusion into an underwater repeater housing is possible if water enters the fiber at a defect site.

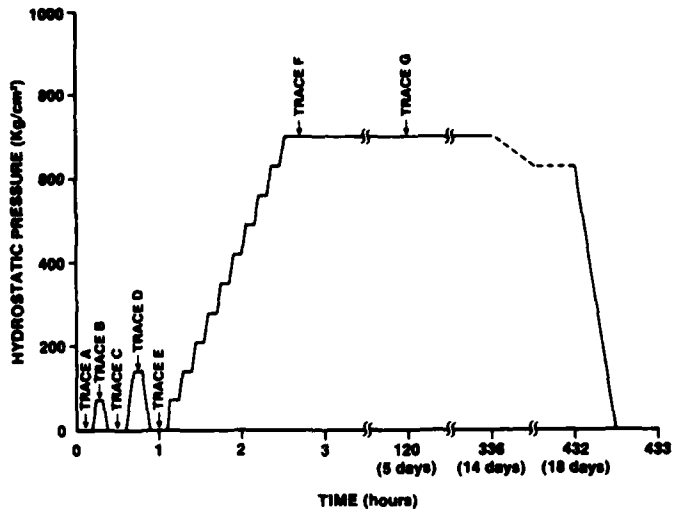

Figure 15. Pressure vs time profile of pressure test.

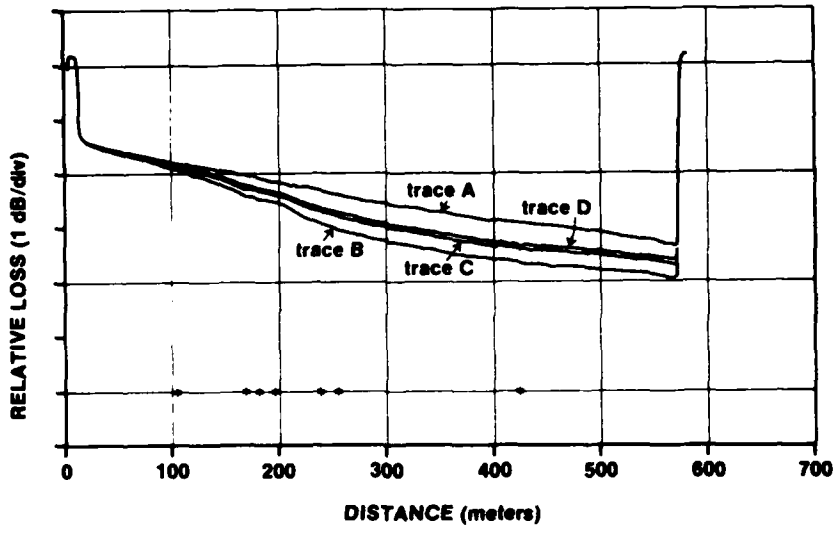

Figure 16. OTDR measurements: traces A, B, C, and D.

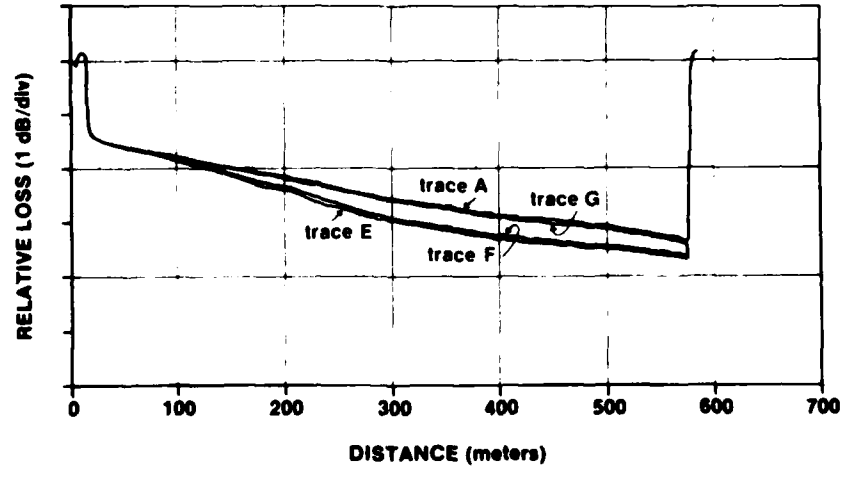

Figure 17. OTDR measurements: traces A, E, F, and G.

PRESSURE SENSITIVITY OF A RUGGEDIZED FIBER

Test Description

Tests performed on a ruggedized fiber described in Figure 18 demonstrated the pressure sensitivity of a fiber ruggedized with an outer jacket of S-glass in an epoxy matrix. This type of ruggedized fiber appears ideal for undersea weapons control or rapidly deployed long-haul links since it is light, small, and nonmetallic. However, the pressure test pointed out the need to reduce pressure sensitivity in fibers ruggedized by means of this technique.

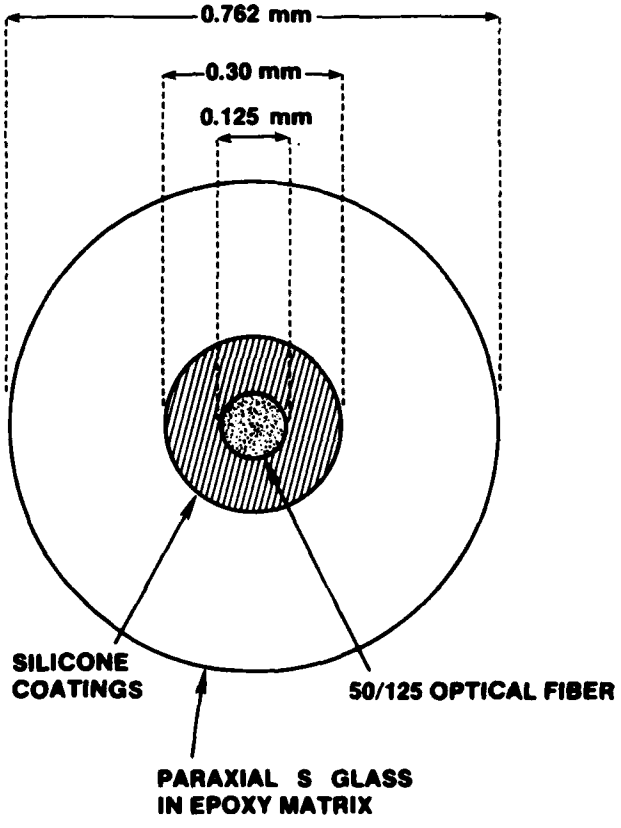

Figure 18. Epoxy/S-glass ruggedized fiber.

This fiber was pressure tested in a 150-m-long linear pressure vessel (Figure 19). The vessel consisted of 0.5-in.-ID high-pressure tubing. This cable was not tested in the 16-in. projectile because the stiffness of the cable made winding it onto the pressure mandrel difficult (Figure 6).

The penetrator (Figure 7) was fabricated in the same manner as the 16-in. projectile. The total fiber length was 250 m. A 150-m length of fiber was tested in the linear vessel and the remaining 100 m served as a "pigtail" between the fiber under test and optical measurement instrumentation. There were no splices in the fiber. The backscatter technique was used to measure pressure-induced excess loss in the fiber.

Figure 19. Linear pressure vessel and controls (foreground).

Pressure Test Results

Pressure on the fiber was cycled four times. Large loss increases were observed in all four pressure cycles. The first three cycles were performed in succession in a single day; the fourth cycle was performed 1-1/2 months after the third. Peak pressures in the first two cycles were 70 kg/cm^2 (1,000 psi) and 140 kg/cm^2 (2,000 psi), respectively. Peak pressures in the third and fourth cycles were 420 kg/cm^2 (6,000 psi). Pressures were limited to 420 kg/cm^2 because presure-induced loss increases for pressure greater than 420 kg/cm^2 were larger than the dynamic range of the OTDR.

Cycle-to-cycle pressure-induced loss increases were not repeatable. This was probably caused by the relatively long stress relaxation time constant of the coating materials. The long time constant caused loss increases to be influenced by the pressure levels in previous cycles. The time constant was estimated to be on the order of several days.

To minimize the influence of the stress relaxation time constant, the fourth pressure cycle was performed 1-1/2 months after the third. Backscatter measurements from the fourth cycle are plotted in Figure 20. Backscatter from the first 100 m of fiber in Figure 20 is from the "pigtail" between the fiber under test and OTDR. Trace A was taken prior to the first cycle and served as the zero-pressure baseline data. The greatest loss increase appears to be between 150 and 175 m into the fiber from the OTDR end. This is indicated by the steep slope of the backscatter traces between these two points. Pressure-induced microbending probably caused this localized loss increase.

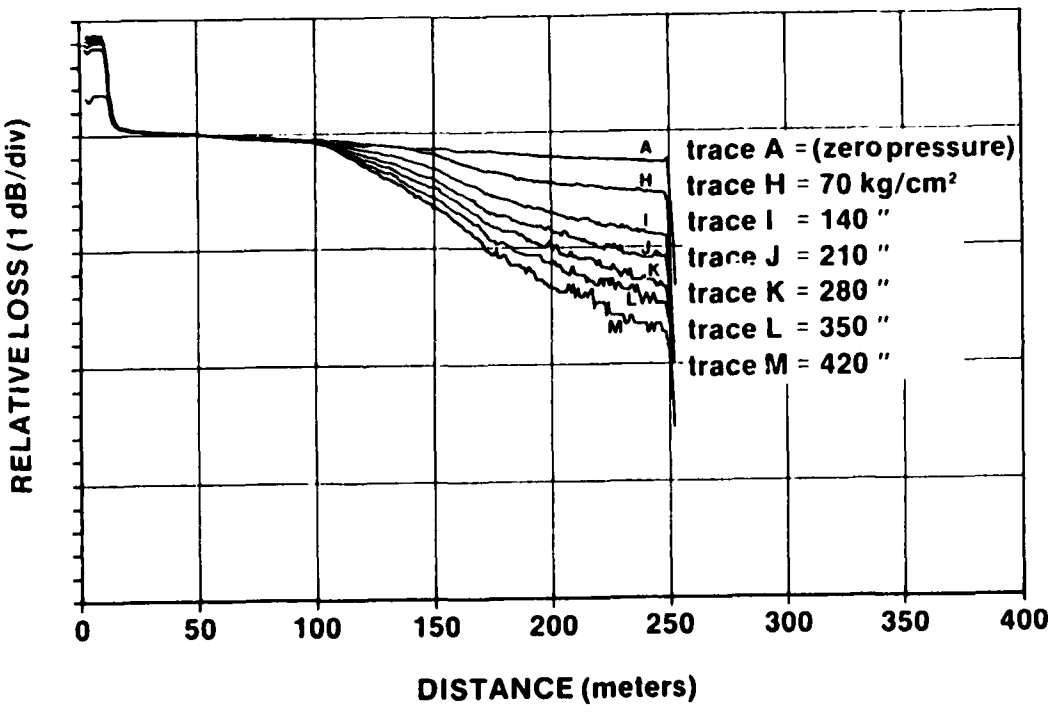

Figure 20. OTDR measurement of epoxy/S-glass-coated fiber under pressure.

The pressure was then increased to 420 kg/cm^2 (6,000 psi), as shown in trace M in Figure 20, and maintained at this level in a long-term soak. The loss increase at this pressure gradually decreased from 7 dB to 3.6 dB after 25 hours. After 178 hours, it decreased to within 1 dB of its original pre-test value. The loss increase gradually dissipated in the high-pressure soak because the coating materials "relaxed" to relieve stresses induced by unbalanced hydrostatic forces. When the pressure on the fiber was released, the fiber loss unexpectedly increased by 1.8 dB. However, losses gradually crept to within 0.3 dB of its pre-test value after 144 hours at atmospheric pressure.

Analysis

This test demonstrated pressure-induced microbending losses in a silicone-coated fiber ruggedized with an epoxy/S-glass outer jacket. Just how the ruggedizing layer contributes to the high sensitivity to pressure is not known exactly. This sensitivity is consistent with the high sensitivity to temperature and excess loss caused by application of the epoxy/S-glass layer. At the same time, the data are inconsistent with tests performed on a Hytrel-coated fiber (same as Fiber B-1 in Table 1) ruggedized with the same epoxy/-S-glass jacket. These tests showed much smaller pressure and temperature sensitivities.

Table 3 summarizes the results of tests performed on the ruggedized fiber. The first row shows the attenuation at a wavelength of 0.83 m before and after application of the epoxy/S-glass jacket over the silicone-coated fiber. An attenuation increase of 2.4 dB/km after the application was measured by Mr. Mike Brininstool of NOSC, San Diego. Application of the epoxy/S-glass also increased the temperature sensitivity of the fiber as indicated in the second row of Table 3. These measurements were performed at both NOSC Hawaii and San Diego with very similar results. The last row in Table 3 lists the results of the pressure tests. In each case, the silicone-coated fiber displayed increased sensitivity to stresses after the epoxy/S-glass jacket was applied.

Table 3. Summary of tests run on silicone-coated fiber and after application of epoxy/S-glass jacket.

MEASUREMENT	SILICONE-COATED FIBER	EPOXY/S-GLASS OVER SILICONE-COATED FIBER
Absolute Loss @ 0.83 μm	3.5 dB/km	5.9 dB/km
Attenuation Increase in Temperature Test	+0.9 dB/km @ -50°C	+59 dB/km @ -50°C
Attenuation Increase in Pressure Test	+0.7 dB/km @ 700 kg/cm^2	+50 dB/km @ 420 kg/cm^2

CONCLUSIONS AND RECOMMENDATIONS

Pressure-induced loss in polymer-coated optical fibers can be avoided by proper choice of coating design parameters and elimination of coating defects. The pressure model in Equation (2) aids in the choice of coating modulus and thickness to minimize axial compression in fibers under pressure. Axial compression is directly proportional to pressure and can lead to buckling of the glass fiber if a compression threshold is exceeded, as shown in Equation (3). Coatings can be designed so that axial compression does not exceed the buckling threshold for pressure less than 700 kg/cm^2 (10,000 psi). If the fiber buckles, it forms a helix inside the coating with small radius of curvature bends. Losses increase as a result of these bends.

The coating must also be free of defects to avoid pressure-induced losses. Even though the coating is designed so that axial compression is less than the buckling threshold, the fiber can still exhibit loss increase if its coating contains defects. Fibers will microbend at coating defect sites at even very low pressures. The obvious solution is to prevent defects by improving quality control during application of the polymer coating. For tough epoxy/S-glass jackets, the cause of pressure sensitivity needs further investigation.

Equation (2) proved to be an adequate pressure model. However, in sea-floor applications, polymer-coated fibers and cables will experience low temperatures as well. Development of a high-pressure, low-temperature model is highly recommended. If axial compressive strain in polymer-coated fibers is the linear sum of pressure-induced strain and temperature-induced strain, the buckling threshold strain may be exceeded. This will result in loss increase. Preliminary experiments on 0.9-mm-OD fibers at 700 kg/cm^2 and 0°C indicate that axial compressive strains may approach the buckling threshold.

REFERENCES

1. M. Kawase, et al., "Optical Loss Change Caused by Hydraulic Pressure in Multimode Optical Fibers," Electronics Letters, vol 15, p 208-209, 29 March 1979.

2. K. Nakagawa, M. Takeshima, and F. Ebisawa, "Hydraulic Pressure Buckling in Plastic Buckling in Plastic Coated Optical Fiber," Electronics Letters, vol 16, p 838-839, 23 October 1980.

3. Y. Katsuyama, et al., "Transmission Loss of Coated Single-Mode Fiber at Low Temperatures," Applied Optics, vol 19, p 4200-4205, 15 December 1980.

4. R. W. Fillers and N. W. Tschoegel, "The Effects of Pressure on the Mechanical Properties of Polymers," Transactions of the Rheology Society, vol 21, p 51-100, 1977.

5. R. Kashyap and M. H. Reeve, "Single-ended Fiber Strain and Length Measurement in Frequency Domain," Electronics Letters, vol 16, p 689-690, 28 August 1980.

6. Naval Ocean Systems Center, Optical Fiber Temperature/Attenuation Studies, by G. A. Wilkins and D. N. Williams, NOSC TD 364, 1 May 1980.

7. N. Yoshizawa, T Yabuta, and K. Noguchi, "Residual Nylon-Jacketed-Fiber Shrinkage Caused by Cooling," Electronics Letters, vol 19, p 411-412, 26 May 1983.

APPENDIX

DERIVATION OF PRESSURE MODEL

The following is a derivation of the pressure model. Axial compression in a polymer-coated fiber is related to pressure, material properties, and fiber dimensions.

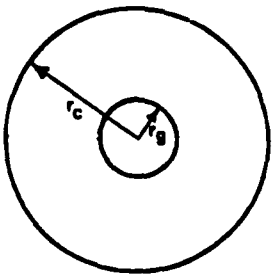

r_g = radius of glass

r_c = radius of coating

use following subscripts:

c = coating
g = glass
x = x axis
y = y axis
z = z axis

use following superscripts:

u = ubonded
b = bonded

Assumption: Assume hydrostatic pressure, p, produced equal triaxial stress in the coating and glass so that

$$\sigma_x, \sigma_y, \sigma_z = p ,$$

where p = pressure, and

$\sigma_x, \sigma_y, \sigma_z$ = stresses in the x, y, z directions, respectively.

This is valid if the coating is softer than glass. The longitudinal elongation for triaxial stress is:

$$\epsilon^u = \frac{p}{E}(1 - 2\nu) = \frac{pk}{3} , \qquad \text{(A-1)}$$

where $\epsilon^u = \frac{\Delta l}{l}$ (unbonded elongation), E = Youngs modulus, ν = Poisson's ratio, and k = compressibility.

If there were no bonding, the coating would shrink more than the glass because it is more compressible. This would produce a gap between the glass and buffer equal to:

$$\text{Gap} = \epsilon_g^u - \epsilon_c^u \quad .$$

For continuity of the bonded connection, there has to be elongation of the coating and compression of the glass fiber such that the sum of these elongations is equal to the unbonded gap. By substitution of (A-1):

$$\epsilon_c^b - \epsilon_g^b = \epsilon_g^u - \epsilon_c^u = \frac{p}{3} \ (K_g - K_c) \qquad \text{(A-2)}$$

By statics, the compressive force must equal the tension. For axial elongation, the forces in the glass and buffer are:

$$F_g = S_g E_g \epsilon_g^b \qquad \text{(A-3)}$$

$$F_c = S_c E_b \epsilon_b^b \qquad \text{(A-4)}$$

so that

$$F_g = -F_c = S_g E_g \epsilon_g^b = -S_b E_b \epsilon_b^b$$

or

$$\epsilon_c^b = \frac{-S_g E_g}{S_c E_c} \epsilon_g^b \quad . \qquad \text{(A-5)}$$

S is the cross-sectional area.

Substituting (A-5) into (A-2) gives

$$\frac{-S_g E_g}{S_c E_c} \epsilon_g^b - \epsilon_q^b = \frac{p}{3} \ (K_g - K_c)$$

or

$$\epsilon_g^b = \frac{\frac{-p}{3} (K_g - K_c)}{\frac{S_g E_g}{S_c E_c} + 1} \quad . \qquad \text{(A-6)}$$

Substituting (A-6) into (A-3) gives

$$F_g = \frac{\frac{-p}{3}(K_g - K_c)\, S_g E_g}{\frac{S_g E_g}{S_c E_c} + 1} = \frac{\frac{-p}{3}(K_g - K_b)}{\frac{1}{S_c E_c} + \frac{1}{S_g E_g}} \qquad \text{(A-7)}$$

Finally, the strain in a coated fiber under pressure is:

$$\epsilon_g = \frac{-p\,(K_g - K_b)}{3\left(1 + \frac{S_g E_g}{S_b E_b}\right)} \quad .$$

END

FILMED

11-85

DTIC